

Chemical Science

Accepted Manuscript

This article can be cited before page numbers have been issued, to do this please use: J. Wu, R. Li, W. Yao, Y. Fu and S. Guo, *Chem. Sci.*, 2026, DOI: 10.1039/D6SC00466K.



This is an Accepted Manuscript, which has been through the Royal Society of Chemistry peer review process and has been accepted for publication.

Accepted Manuscripts are published online shortly after acceptance, before technical editing, formatting and proof reading. Using this free service, authors can make their results available to the community, in citable form, before we publish the edited article. We will replace this Accepted Manuscript with the edited and formatted Advance Article as soon as it is available.

You can find more information about Accepted Manuscripts in the [Information for Authors](#).

Please note that technical editing may introduce minor changes to the text and/or graphics, which may alter content. The journal's standard [Terms & Conditions](#) and the [Ethical guidelines](#) still apply. In no event shall the Royal Society of Chemistry be held responsible for any errors or omissions in this Accepted Manuscript or any consequences arising from the use of any information it contains.

EDGE ARTICLE

Point-to-Volume Engineering Enables Enhanced Birefringence and Wide Bandgap in Hybrid Halide Ultraviolet Nonlinear Optical Crystals

Jiajing Wu,^a Ruo-Nan Li,^a Wen-Dong Yao,^a Yi-Fan Fu, Sheng-Ping Guo^{*a,b}Received 00th January 20xx,
Accepted 00th January 20xx

DOI: 10.1039/x0xx00000x

Ultraviolet nonlinear optical (UV NLO) crystals are important for advanced photonics, yet their development is hindered by the inherent trade-off among strong SHG response, wide bandgap and large birefringence. Herein, guided by systematic theoretical screening, the “two-in-one” flexible π -conjugated (C₄H₁₃N₅)²⁺ (**MF**) group was identified as a prospective functional building unit (FBU) owing to its superior polarizability anisotropy and hyperpolarizability. Its initial combination with Cl⁻ yielded C₄H₁₃N₅Cl₂ (**MFC**), which exhibits a wide band gap (4.64 eV) and a high SHG response (2.8 × KH₂PO₄ (KDP)), yet with a small birefringence of 0.02@546 nm. To address this limitation, we implemented a point-to-volume substitution strategy, replacing the discrete Cl⁻ anions in MFC with distorted [ZnCl₄]²⁻ tetrahedra, yielding a novel zero-dimensional (0D) organic-inorganic hybrid halide (C₄H₁₃N₅)ZnCl₄ (**MFZC**). This structural evolution simultaneously enhances most of key optical properties: bandgap widening to 4.72 eV, birefringence enhancement to 0.09 at 546 nm, and retention of a strong SHG response of 2.2 × KDP. Theoretical and structural analyses indicate that the improved properties originate from the synergistic alignment of organic **MF** cations and inorganic [ZnCl₄]²⁻ tetrahedra FBU. This work provides an effective strategy for engineering hybrid halide materials with concurrently optimized linear and nonlinear optical properties.

Introduction

Nonlinear Optical (NLO) crystals are indispensable for frequency conversion in solid-state lasers,^{1,2} enabling the generation of coherent light and extending the operational wavelength into the short-wavelength ultraviolet (UV) region.^{3–5} Their functionality is critical for key applications including precision micromachining, modern medical treatment, and information storage.^{6–9} However, high-performance commercial UV NLO materials are rather scarce, with representative ones including β -BaB₂O₄ (β -BBO),¹⁰ LiB₃O₅ (LBO),¹¹ and KBe₂BO₃F₂ (KBBF).¹² Excellent UV NLO materials must achieve an effective balance among large second-harmonic generation (SHG) effects, wide bandgap and appropriate birefringence.^{13–15} These properties, however, are mutually constrained, making their concurrent optimization within a single crystal a persistent challenge. To achieve balance, researchers are paying increasing attention to the rational structure design of such materials.¹⁶

The rational design of structural motifs and the deliberate choice of their assembly modes serve as the key background for optimizing NLO properties. Inorganic π -conjugated groups,

such as (BO₃)³⁻,¹⁷ (NO₃)⁻,¹⁸ and (B₃O₆)³⁻,¹⁹ serve as superior UV NLO-active building units and exhibit strong polarizability anisotropy (δ) and large hyperpolarizability tensor ($\beta_{|max|}$). These features have enabled the development of notable NLO crystals, including KBBF,¹² RE(OH)₂NO₃ (RE = La, Y, Gd),²⁰ and Ba₂Mg(B₃O₆)₂ (BMBO).²¹ However, the growth of inorganic NLO crystals is typically associated with high costs, substantial energy consumption, and prolonged processing times.²² Studies have shown that organic π -conjugated groups such as (C₃N₃S₃H_x)^{x-3} ($x = 0–3$),^{23–26} [C(NH₂)₃]⁺ (Gua⁺),^{2,27} and (DAMS⁺)²⁸ etc, outperform their structurally similar inorganic counterparts in both second-order polarizability and optical anisotropy.¹⁶ For example, the large delocalized π -electron systems of Cd(SCN)₂(C₄H₆N₂)₂ (10 × KDP, E_g = 4.74 eV),²⁹ ZnBr(C₆H_{3.5}FNO₂)₂ (1.7 × KDP, E_g = 4.2 eV),³⁰ (C₅H₆N₂O₂)ZnCl₂ (3.5 × KDP, E_g = 5.19 eV),³¹ and [C(NH₂)₃]₃PO₄·2H₂O (1.5 × KDP, E_g = 4.2 eV)² can effectively balance the critical performance metrics indispensable for short-wave UV NLO crystals.

The coupling of functional groups (e.g., dimeric [B₂O₅]⁴⁻ and [P₂O₇]⁴⁻) is recognized as an effective strategy for enhancing SHG efficiency.³² However, achieving precise and controllable coupling in inorganic systems remains synthetically challenging,³³ whereas such coupling can be more readily and predictably realized in organic frameworks.³⁴ Taking examples such as M₄Mg₄(P₂O₇)₃ (M = K, Rb),³³ NH[C(NH₂)₂]₂(NO₃)₂,¹⁶ {N[C(NH₂)₂]₂CO₃},¹⁶ and [C₂N₄H₇O][NH₂SO₃],³² and inspired by this, we have identified such a flexible “two-in-one” configuration organic groups, metformin [(C₄H₁₃N₅)²⁺, abbreviated **MF**], which is formed by combination of planar [C(NH₂)₃]⁺ and [C(NH₂)₃(CH₃)₂] via sharing a nitrogen atom.

^a *School of Chemistry and Materials, Yangzhou University, Yangzhou, Jiangsu 225002, P. R. China.

^b *School of Materials and Energy, Yunnan University, Kunming 650500, P. R. China.

E-mail: spguo@yzu.edu.cn, jiajingw@yzu.edu.cn.

††Electronic Supplementary Information (ESI) available: Additional tables and pictures. CCDC: 2521794, 2522224 See DOI: 10.1039/x0xx00000x



Theoretical calculations reveal that the π -conjugated **MF** cation exhibits favorable δ values and a large β_{max} , exceeding those of well-known building units such as $[\text{BO}_3]^{3-}$,¹⁷ $(\text{NO}_3)^-$,¹⁸ $(\text{C}_2\text{N}_4\text{OH}_7)^+$,³² etc. (Fig. 1). These results demonstrate that the **MF** moiety represents a highly promising functional building block for the design of nonlinear optical crystals.

Based on the anionic group theory,³⁵ the rational introduction of halide anions or their assembled metal-halide polyhedral units serves as a key molecular design strategy for developing high-performance NLO crystals. Halide anions (Cl^- , Br^- , I^-), with their high electronegativity and strong polarizability, can effectively widen the optical bandgap and enhance the macroscopic polarization of the crystal lattice, such as $\text{Mg}_2\text{PO}_4\text{Cl}$,³⁶ $\text{Ba}_3\text{P}_3\text{O}_{10}\text{Cl}$.³⁷ When coordinated with metal cations with stereochemically active lone pairs (Pb^{2+} , Sb^{3+} , Te^{4+}) or d^{10} electron configurations (Cd^{2+} , Zn^{2+}), they form structurally distorted metal-halogen polyhedra, which not only break the structural symmetry but also provide large microscopic second-order susceptibility. Examples include $(\text{L-ipp})(\text{L-pro})\text{PbI}_3$,³⁸ $(\text{C}_5\text{H}_6\text{N}_2\text{O}_2)\text{ZnBr}_2$,³¹ and $[\text{DASH}]\text{Cd}_2\text{Cl}_6$.²⁸

Guided by this strategy, we have successfully synthesized $\text{C}_4\text{H}_{13}\text{N}_5\text{Cl}_2$ (**MFC**) through the rational integration of the distinctive merits of organic cations $(\text{C}_4\text{H}_{13}\text{N}_5)^{2+}$ (**1**) (Fig. 1). Although **MFC** was initially reported in 2023,³⁹ its optical properties have not yet been systematically investigated. Meanwhile, by employing a novel point-to-volume substitution strategy—replacing the discrete Cl^- ions in **MFC**

with $[\text{ZnCl}_4]^{2-}$ tetrahedral units—we have obtained a new UV NLO crystal $(\text{C}_4\text{H}_{13}\text{N}_5)\text{ZnCl}_4$ (**MFZC**). Both **MFC** and **MFZC** exhibit wide bandgaps (> 4.6 eV) and strong SHG responses ($> 2 \times \text{KDP}$). Notably, the birefringence value of **MFZC** exhibits a 4.5 times enhancement relative to that of **MFC** because **MFZC** features a significantly higher degree of structural ordering compared with **MFC**. Here, we present a systematic investigation into the synthesis, crystal structures, optical properties, theoretical calculations, and structure-property relationships of **MFC** and **MFZC**.

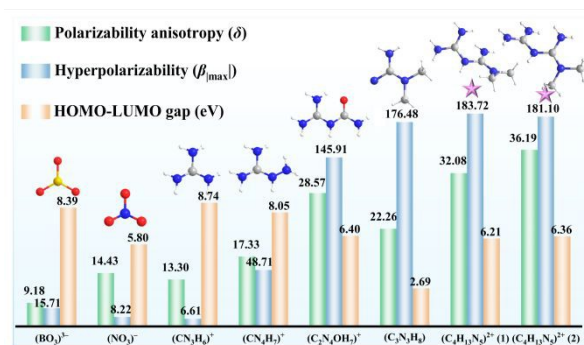


Fig. 1 Calculated gaps between the highest occupied molecular orbital (HOMO) and the lowest unoccupied molecular orbitals (LUMO), polarizability anisotropy (δ), and the maximum absolute value of hyperpolarizability (β_{max}) of typical functional groups.

Results and discussion

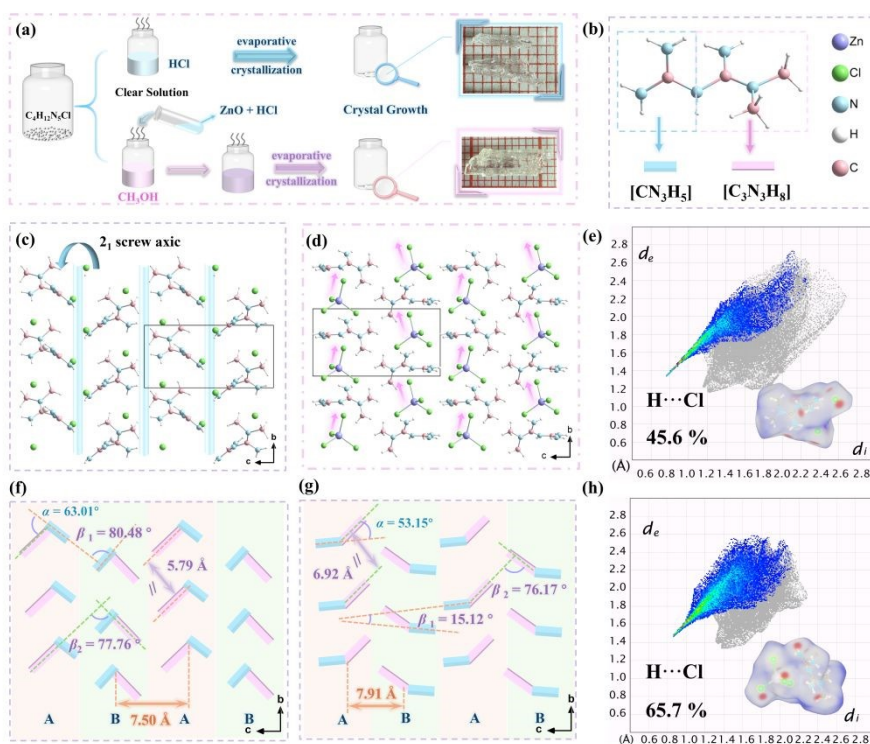


Fig. 2 (a) The synthesis of **MFC** and **MFZC**. (b) Functional motifs in **MF**. The crystal structures of (c) **MFC** and (d) **MFZC**. Hirshfeld surfaces for (e) **MFC** and (h) **MFZC**. Modular description of functional motifs for (f) **MFC** and (g) **MFZC**.

The colorless and transparent crystals of **MFC** (rod-shaped) and **MFZC** (block-shaped) were obtained via slow solvent evaporation at room temperature (Fig. 2a). Their crystal structures were confirmed by single-crystal X-ray diffraction (SCXRD) analysis, and detailed crystallographic data are summarized in Tables S1–S5 (Supporting Information). Both

MFC and **MFZC** crystallize in the monoclinic polar noncentrosymmetric (NCS) space group $P2_1$ (No. 4), and feature zero-dimensional (0D) structural (Fig. 2c and 2d). The phase purities of **MFC** and **MFZC** were confirmed by powder X-ray diffraction (PXRD) analysis (Fig. S1).



For **MFC**, its asymmetric unit contains one protonated **MF** cation and two free Cl^- anions (Fig. S2). The **MF** unit exhibits a “two-in-one” flexible configuration, comprising planar $[\text{CN}_3\text{H}_5]$ and $[\text{C}_3\text{N}_3\text{H}_8]$ groups (Fig. 2b). The dihedral angle between them, denoted as α , is 63.01° in **MFC**. As shown in Fig. S3, the organic **MF** molecules and Cl^- anions are interconnected via hydrogen bonds in the *ab*-plane, forming a *pseudo-2D* structure. The layers stack along the *c*-axis, resulting in a *pseudo-3D* network framework. Along the *c*-axis, the organic molecules **MF** exhibit an alternating –ABAB– arrangement. The dihedral angles between adjacent organic cations in layer A and layer B were determined to be $\beta_1 = 80.48^\circ$ (between two $[\text{CN}_3\text{H}_5]$ planes) and $\beta_2 = 77.76^\circ$ (between two $[\text{C}_3\text{N}_3\text{H}_8]$ planes), respectively, with an interlayer distance of 7.50 \AA (Fig. 2f). Within layer A or layer B, adjacent organic cations aligned along the *b*-axis exhibit a dihedral angle of 0° and an interatomic spacing of 5.79 \AA (Fig. 2f). The organic **MF** cation is off the (001) crystal plane with a dihedral angle (γ) of 86.37° (Fig. S7a). To further evaluate the interplay of molecular interactions in the structure of **MFC**, we employed Hirshfeld surface (HS) analysis and mapped the d_{norm} , which are presented in Fig. 2e. The red areas on the Hirshfeld surface correspond to significant $\text{H}\cdots\text{Cl}$ contacts (Fig. 2e). The percentage contribution of $\text{H}\cdots\text{Cl}$ interaction is 45.6% for **MFC** (Fig. 2e and S6a).

In contrast to **MFC**, the Cl^- anions in **MFZC** are not free ions but coordinate to Zn atoms, forming tetrahedral $[\text{ZnCl}_4]^{2-}$ units. The asymmetric unit of **MFZC** consists of one such $[\text{ZnCl}_4]^{2-}$ tetrahedron and one protonated **MF** cation (Fig. S4). The

dihedral angle (α) within the **MF** unit decreases from 63.01° to 53.15° . **MFZC** also adopts a *pseudo-layered* structure parallel to the *ab* plane, wherein the $(\text{C}_4\text{H}_{13}\text{N}_5)^{2+}$ cations and $[\text{ZnCl}_4]^{2-}$ anions are interconnected by $[\text{N}\cdots\text{Cl}]$ and $[\text{C}\cdots\text{Cl}]$ hydrogen bonds, with the $\text{H}\cdots\text{Cl}$ distances ranging from 2.47 to 2.79 \AA (Fig. S5 and Table S5). These *pseudo*-layers stack along the *c* direction to form the entire 3D network of **MFZC** (Fig. S5). Similar to **MFC**, the organic moieties **MF** in **MFZC** adopt an alternating “ABAB” arrangement along the *c*-axis, with an interlayer distance of 7.91 \AA (Fig. 2g). Notably, within the organic **MF** cations in **MFZC**, the $[\text{C}_3\text{N}_3\text{H}_8]$ adopts a *zig-zag* arrangement with $\beta_2 = 76.17^\circ$, whereas $[\text{CN}_3\text{H}_5]$ groups exhibit $\beta_1 = 15.12^\circ$ and interatomic spacing of 6.92 \AA . The $\text{H}\cdots\text{Cl}$ ratio of these hydrogen bonds is higher in **MFZC** than in **MFC** (Fig. 2e and 2h). These enhanced hydrogen-bonding interactions impose strong structural constraints on the cationic framework, effectively restricting the relative orientation between adjacent organic planes and reducing the dihedral angles. This ordered alignment significantly enhances the overall birefringence of **MFZC** (Fig. 2g). Additionally, the **MF** cations are oriented off the (001) crystal plane with a dihedral angle of $\gamma_2 = 80.28^\circ$ for **MFZC**, which is smaller with that of **MFC** ($\gamma_1 = 86.37^\circ$) (Fig. S7b). This structural feature further enhances optical anisotropy of **MFZC**. The red regions in the 2D fingerprint plots of hydrogen bonds correspond to $\text{H}\cdots\text{Cl}$ contacts, accounting for 65.7% of the total interaction. This proportion, which is greater than **MFC** (45.6%), underscores the critical role of hydrogen bonds in stabilizing the structure framework (Fig. 2h and S6b).

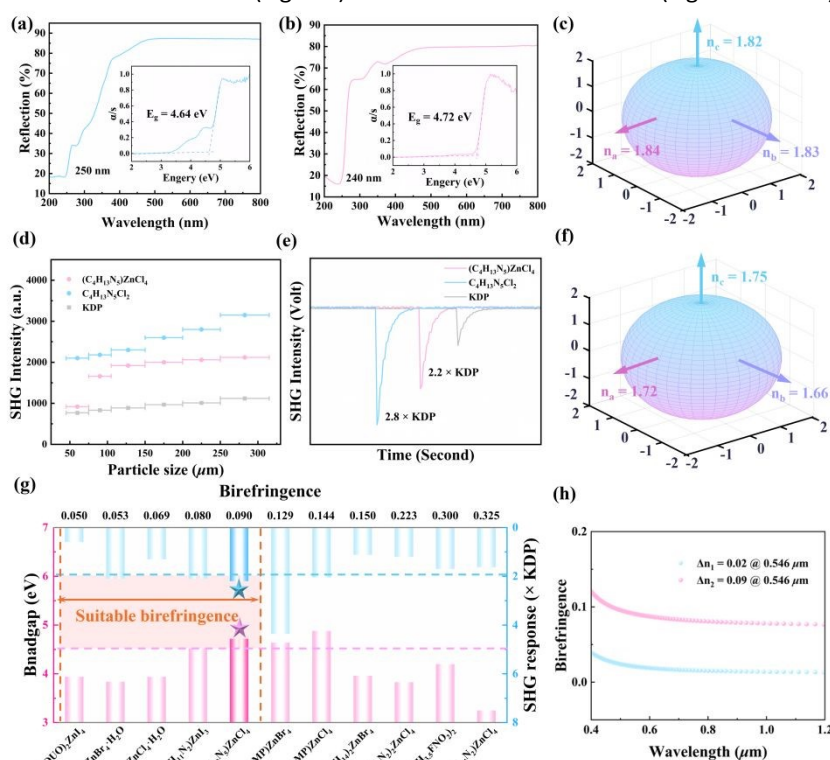


Fig. 3 (a, b) UV-vis spectra of **MFC** (a) and **MFZC** (b). (c, f) Triaxial ellipsoid of three principal refractive indices at 546 nm for (c) **MFC** and (f) **MFZC**. (d) Size-dependent SHG responses of **MFC**, **MFZC** and KDP under 1064 nm laser radiation. (e) SHG intensities of **MFC**, **MFZC** and KDP at 1064 nm. (g) Comparison of bandgap, SHG efficiency and birefringence in organic-inorganic hybrid zinc-based materials. (h) The calculated birefringences of **MFC** and **MFZC**.

The UV-vis-NIR diffuse reflectance spectra demonstrate that the UV cutoff edge of **MFC** is located at 250 nm, while **MFZC** shows a blue-shifted edge at approximately 240 nm (Fig. 3a and

3b). The corresponding optical bandgap values were determined to be 4.64 eV for **MFC** and 4.72 eV for **MFZC**, consistent with the colorless and transparent appearance of the



crystals (Fig. 2a). Notably, the bandgap of **MFZC** surpasses previously reported hybrid Zn-based halide NLO crystals including (4-AMP)ZnX₄·H₂O (X = Cl, Br),⁵ (3-AMP)ZnBr₄,⁴⁰ (C₄H₁₁N₂)ZnI₃,⁴¹ and (C₆H₅N₂)₂ZnCl₄.⁴² The NCS structures of **MFC** and **MFZC** motivated the evaluation of their SHG responses at 1064 nm using the Kurtz–Perry method,⁴³ with commercially available KDP serving as the reference. As shown in Fig. 3d and 3e, **MFC** and **MFZC** exhibit strong SHG responses, reaching 2.8 × and 2.2 × KDP, respectively. Furthermore, as the particle size increases, their SHG intensities increase significantly, indicating that they both exhibit phase-matching behaviors. Notably, **MFC**

demonstrates more outstanding SHG properties than the majority of metal-free materials, such as C₁₂H₉N₃O₄,⁴⁴ C(NH₂)₃(I₃O₈)(Hl₃O₈)(H₂I₂O₆)(HlO₃)₄·3H₂O⁴⁵ and [C₅H₆O₂N₃]₂[IO₃]₂.⁴⁶ In addition, **MFZC** demonstrates better SHG performance than most similar organic–inorganic zinc-based hybrid materials, like (C₁₄H₁₄N₂)ZnCl₄,⁴⁷ (C₆H₁₆N₂)₃Zn₃Br₁₂·2H₂O,⁴⁸ (C₄H₁₁N₂)ZnCl₃,⁴¹ and (C₁₃N₃H₁₄)₂ZnBr₄.⁴⁹ (Fig. 3g and Table S6). The wide bandgaps and strong SHG responses of **MFC** and **MFZC** make them promising UV NLO crystals.

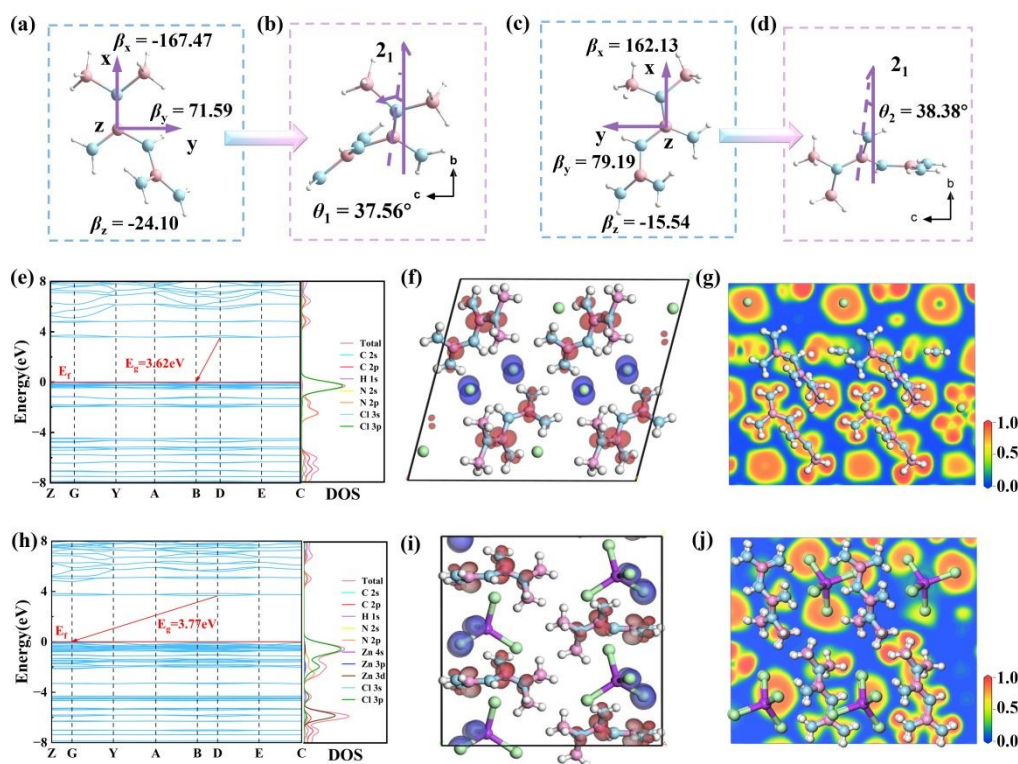


Fig. 4 (a, c) Distribution of the first hyperpolarizabilities of organic cations **MFC** and **MFZC**, respectively. Angle (θ) between the θ_{\max} vector and the crystal polar 2_1 axis in **MFC** (b) and **MFZC** (d). Calculation results: (e, h) Calculated band structure and DOS diagrams of (e) **MFC** and (h) **MFZC**. (f, i) The HOMO (blue sector) and LUMO (red sector) maps of (f) **MFC** and (i) **MFZC**. (g, j) The ELF diagrams of (g) **MFC** and (j) **MFZC**.

To clarify structure–property relationships of **MFC** and **MFZC**, the hyperpolarizability of organic moieties and density functional theory (DFT) calculations were conducted. The organic moieties in **MFC** and **MFZC** exhibit the anticipated anisotropy in polarizability, and their hyperpolarizabilities follow the descending order of $\beta_x > \beta_y > \beta_z$ (Fig. 4a and 4c). As **MFC** and **MFZC** are polar crystals, their polar axes are aligned parallel to the crystallographic b -axis along the 2_1 screw axis, a feature dictated by the symmetry of their crystal structures. Consequently, the combined polarizability components along the 2_1 screw axis contribute to the second-order nonlinear optical response.⁵⁰ As illustrated in Fig. 4b and 4d, the hyperpolarizability components of **MFC** and **MFZC** along the 2_1 screw axis yield values of $\theta_1 = 37.56^\circ$ and $\theta_2 = 38.38^\circ$, respectively. Furthermore, compared with **MFZC**, **MFC** exhibits a larger hyperpolarizability of the organic (C₄H₁₃N₅)²⁺ molecules (Fig. 1), together with larger dihedral angles β_1 and β_2 between adjacent layers ($\beta_1 = 80.48^\circ$ and $\beta_2 = 77.76^\circ$ for **MFC**, $\beta_1 = 15.12^\circ$ and $\beta_2 = 76.17^\circ$ for **MFZC**) (Fig. 2). These factors collectively contribute to the slightly higher SHG intensity of **MFC** relative to **MFZC**.

Meanwhile, the electronic structure analysis indicates that both **MFC** and **MFZC** exhibit indirect bandgaps, with calculated values of 3.62 eV for **MFC** and 3.77 eV for **MFZC** (Fig. 4e and 4h), where the a little underestimation relative to experimental values is attributed to the well-known limitation of the generalized gradient approximation (GGA) in treating exchange–correlation energy discontinuities.^{51,52} Since the optical properties of crystalline materials are predominantly determined by electronic transitions near the band edges, we analyzed their total (TDOS) and partial density of states (PDOS) near the Fermi level ($E_f = 0$ eV). The results show that the valence band maximum (VBM) of **MFC** is dominated by Cl 3p states, while that of **MFZC** receives additional contribution from Zn 3d orbitals. In contrast, the conduction band minimum (CBM) of both compounds is primarily composed of C 2p and N 2p states from the organic **MF** cation. Therefore, the linear and nonlinear optical properties of **MFC** and **MFZC** arise from the synergistic interplay between their organic and inorganic components. This conclusion is further corroborated by frontier molecular orbital analysis (Fig. 4f and 4i): the highest occupied



molecular orbital (HOMO) is localized on Cl atoms in **MFC** and extends on both Zn 3d and Cl 3p in **MFZC**, whereas the lowest unoccupied molecular orbital (LUMO) in both compounds is dominated by the C 2p and N 2p orbitals of the organic **MF** cation. To gain an in-depth understanding of the microscopic mechanism underlying the NLO properties, the maps of electron localization function (ELF) were studied (Fig. 4g and 4j). Notably, the electron cloud density around **MF** in **MFC** and **MFZC** exhibits obvious π -conjugated structural features. In addition, there is a significant electron cloud distribution around the Cl⁻ ions in **MFC** and **MFZC**. Consequently, the **MF** cations and Cl⁻/[ZnCl₄]²⁻ anions significantly contribute to their linear and nonlinear optical properties.

The birefringences of **MFC** and **MFZC** were further evaluated through the first-principles theoretical calculations (Fig. S8 and S9). At 546 nm, the three principal refractive indices of **MFC** and **MFZC** are illustrated in Fig. 3c and 3f. Specifically, the refractive indices of **MFC** follow the order of $n_a > n_b > n_c$, whereas those of **MFZC** exhibit the sequence $n_c > n_a > n_b$. Their birefringences are calculated to be 0.02 and 0.09 at 546 nm, respectively (Fig. 3h). It is worth noting that the birefringence of **MFZC** is 4.5 times higher than that of **MFC**, owing to (i) The organic (C₄H₁₃N₅)²⁺ cations of **MFZC** possess a larger polarizability anisotropy than those of **MFC** (Fig. 1). (ii) The dihedral angle (α) within the **MF** moiety decreases from 63.01° in **MFC** to 53.15° in **MFZC**. (iii) The dihedral angles between adjacent organic cations in the A and B layers of **MFC** are determined to be $\theta_1 = 80.48^\circ$ and $\theta_2 = 77.76^\circ$, respectively. In contrast, for the organic **MF** cations in **MFZC**, the corresponding dihedral angles are $\theta_1 = 15.12^\circ$ and $\theta_2 = 76.17^\circ$ (Fig. 2). (iv) The **MF** cation exhibits an orientation deviation from the (001) plane, with the dihedral angle $\gamma_2 = 80.28^\circ$ for **MFZC** being lower than $\gamma_1 = 86.37^\circ$ for **MFC** (Fig. S7). Furthermore, the birefringence of **MFZC** is larger than those of some commercial crystals and zinc-based hybrid halide crystals, such as MgF₂ ($\Delta n = 0.012@532$ nm),⁵³ LiNbO₃ (0.089@546 nm),⁵⁴ and (4-AMP)ZnX₄·H₂O (X = Cl, Br) (0.069@546 nm, 0.053@546 nm, respectively).⁵ Therefore, these data demonstrate that the birefringences of **MFC** and **MFZC** are predominantly governed by **MF** moieties, highlighting that the coupling of π -conjugated groups represents a meaningful strategy for manipulating the macroscopic optical anisotropy of materials.

Conclusions

In conclusion, this work demonstrates that the metformin cation **MF** is a promising NLO-active functional motif and reports the synthesis of new **MFZC** via a point-to-volume substitution strategy from **MFC**. **MFZC** exhibits strong SHG response and wide optical bandgap. Moreover, the successful introduction of [ZnCl₄]²⁻ tetrahedral units and the favorable arrangement of organic cations collectively enhance the optical anisotropy of **MFZC**, much higher than that of **MFC**. Theory calculation and structural analysis demonstrate that the optical properties of **MFC** and **MFZC** are synergistically affected by both organic **MF** cation and inorganic halogen ions/metal-halide anions. This work offers not only a promising UV NLO material, but also an effective strategy for the rational design of novel SHG materials.

Data availability

All the supporting data associated with this work are available in the ESI.†

DOI: 10.1039/D6SC00466K

Author Contributions

This work was conceptualized by Jiajing Wu. Experimentation was performed by Ruo-Nan Li. Software analysis was performed by Wen-Dong Yao. Besides, Jiajing Wu and Sheng-Ping Guo contributed to funding acquisition and supervision. The first draft of the manuscript was prepared by Jiajing Wu and Ruo-Nan Li, and the final draft was edited by all the authors.

Conflicts of interest

The authors declare that they have no conflict of interest.

Acknowledgements

This work was supported by the National Natural Science Foundation of China (22505217, 22371246), Natural Science Foundation of Jiangsu Province (Grant No. BK20220558), Yangzhou University Science and Technology Innovation Fund (2022CXJ029), Yangzhou University with a start-up fund (Grant No. 137012279) and the Lvyangjinfeng Talent Program of Yangzhou (YZLYJFJH2021YXBS085).

Notes and references

- S. Zhao, P. Gong, L. Bai, X. Xu, S. Zhang, Z. Sun, Z. Lin, M. Hong, C. Chen, J. Luo, *Nat. Commun.*, 2014, **5**, 4019.
- X. Wen, C. Lin, M. Luo, H. Fan, K. Chen, N. Ye, *Sci. China Mater.*, 2021, **64**, 2008–2016.
- D. F. Eaton, *Science*, 1991, **253**, 281–287.
- N. Savage, *Ultraviolet Lasers*, *Nat. Photonics.*, 2007, **1**, 83–85.
- C. Shen, C. Zhang, Q. Xing, D. Sun, K. Wu, B. Zhang, J. Wang, D. Wang, *Chem. Eng. J.*, 2025, **509**, 161389.
- H. Fan, N. Ye, M. Luo, *Acc. Chem. Res.*, 2023, **56**, 3099–3109.
- S. Choi, Y. Li, Y. Kuk, K. M. Ok, *Adv. Sci.*, 2025, **12**, 2414503.
- Z. Chen, C. Liu, C. Li, J. Lu, Z. Yang, S. Pan, M. Mutailipu, *Adv. Opt. Mater.*, 2025, **13**, 2500631.
- K. M. OK, *Acc. Chem. Res.*, 2016, **49**, 2774.
- J. Lin, M. Lee, Z. Liu, C. Chen, C. Pickard, *Phys. Rev. B.*, 1999, **60**, 13380.
- C. Chen, Y. Wu, A. Jiang, B. Wu, G. You, R. Li, S. Lin, *J. Opt. Soc. Am. B.*, 1989, **6**, 616.
- C. T. Chen, G. L. Wang, X. Y. Wang, Z. Y. Xu, *Appl. Phys. B.*, 2009, **97**, 9–25.
- P. S. Halasyamani and J. M. Rondinelli, *Nat. Commun.*, 2018, **9**, 2972.
- Y.-F. Fu, W.-D. Yao, Q.-F. Huang, S.-F. Yan, W. Liu, J. Wu, *Inorg. Chem.*, 2025, **64**, 15813–15817.
- Y.-F. Fu, W.-D. Yao, J. J. Wu, Q.-F. Huang, Y.-M. Zhang, W. Zhou, W. Liu, S.-P. Guo, *Small*, 2025, **21**, 2412173.
- Y. Zhang, Q. Ding, Y. Li, Y. Li, X. Song, W. Huang, Y. Zhou, Q. Shao, Z. Bai, S. Zhao, J. Luo, *Laser Photonics Rev.*, 2025, **19**, 2500368.



17. Y. Liu, X. Liu, S. Liu, Q. Ding, Y. Li, L. Li, S. Zhao, Z. Lin, J. Luo, M. Hong, *Angew. Chem. Int. Ed.*, 2020, **59**, 7793–7796.
18. F. Kong, C.–L. Hu, M.–L. Liang, J.–G. Mao, *Inorg. Chem.*, 2016, **55**, 948–955.
19. H. Wu, Z. Wei, Z. Hu, J. Wang, Y. Wu, H. Yu, *Angew. Chem. Int. Ed.*, 2024, **63**, e202406318.
20. Y. Song, M. Luo, C. Lin, N. Ye, *Chem Mater.*, 2017, **29**, 896–903.
21. R. K. Li and Y. Ma, *CrystEngComm*, 2012, **14**, 5421–5424.
22. K. Yang, D. Wang, C. Zhu, K. Wu, G. Liu, J. Wang, C. Shen, *Mater. Today Chem.*, 2025, **48**, 102916.
23. X. Hao, C. S. Lin, M. Luo, Y. Q. Zhou, N. Ye, E. Shangguan, *Inorg. Chem.*, 2023, **62**, 7611–7616.
24. X. Hao, C. S. Lin, N. Ye, D. H. Lin, D. Zhao, Y. Q. Zhou, E. Shangguan, M. Luo, *Cryst. Growth Des.*, 2023, **23**, 362–368.
25. J. M. Zhao, H. K. Liu, X. D. Zhang, B. B. Zhang, Y. Wang, *CrystEngComm.*, 2020, **22**, 6495–6501.
26. M. J. Li, X. Zhang, Z. Y. Xiong, Y. Q. Li, Y. Zhou, X. Chen, Y. P. Song, M. C. Hong, J. H. Luo, S. G. Zhao, *Angew. Chem. Int. Ed.*, 2022, **61**, e202211151.
27. M. Mutailipu, J. Han, Z. Li, F. Li, J. Li, F. Zhang, X. Long, Z. Yang, S. Pan, *Nat. Photonics.*, 2023, **17**, 694–701.
28. Y. Wu, Y. Li, Y. Zhang, B. Teng, X. Jiang, C. Hu, S. Sun, L. Cao, J. Ma, K. Xu, D. Xu, Z. Lin, D. Zhong, *Adv. Funct. Mater.*, 2025, **35**, 2503125.
29. Y. Kang, C. Yang, J. Gou, Y. Zhu, Q. Zhu, W. Xu, Q. Wu, *Angew. Chem. Int. Ed.*, 2024, **63**, e202402086.
30. Q. Zhu, Y. Tao, C. Yang, J. Gou, Y. Zhu, X. Wang, Q. Wu, *Inorg. Chem.*, 2024, **63**, 22620–22627.
31. Y. Zhu, J. Gou, C. Yang, Q. Zhu, Y. Xiong, Q. Wu, *Angew. Chem. Int. Ed.*, 2025, **64**, e202509290.
32. X. Wen, Y. Yan, J. Lu, X. Shi, P. Tang, J. Chen, G. Yang, G. Peng, H. Yu, H. Zhang, Z. Hu, J. Wang, N. Ye, *Angew. Chem. Int. Ed.*, 2025, **64**, e202424153.
33. H. Yu, J. Young, H. Wu, W. Zhang, J. M. Rondinelli, P. S. Halasyamani, *Chem. Mater.*, 2017, **29**, 1845–1855.
34. P. Wang, Q. Huang, X. Meng, L. Liu, Q. Wu, H. Liu, *Inorg. Chem. Front.*, 2026, DOI: 10.1039/d5qi02396c.
35. C. T. Chen, Y. C. Wu and R. K. Li, *Int. Rev. Phys. Chem.*, 1989, **8**, 65–91.
36. J. X. Zhang, Q. G. Yue, S. H. Zhou, X. T. Wu, H. Lin, Q. L. Zhu, *Angew. Chem., Int. Ed.*, 2024, **63**, e202413276.
37. P. Yu, L.–M. Wu, L.–J. Zhou, L. Chen, *J. Am. Chem. Soc.*, 2014, **136**, 480.
38. J. Cheng, G. Yi, Z. Zhang, Y. Long, H. Zeng, L. Huang, G. Zou, Z. Lin, *Angew. Chem. Int. Ed.*, 2024, **63**, e202318385.
39. Y.–P. Xia, *N. Cryst. Struct.*, 2023, **238**, 799–800.
40. C. Shen, J. Liu, D. Sun, K. Yang, B. Zhang, K. Wu, J. Wang, D. Wang, *Small*, 2025, **21**, 2501471.
41. J. Chen, H.–Y. Wu, M.–B. Xu, M.–C. Wang, Q.–Q. Chen, B.–X. Li, C.–L. Hu, K.–Z. Du, *Inorg. Chem. Front.*, 2024, **11**, 5587–5597.
42. D.–X. Yang, Y.–L. Lv, J.–D. Guo, W.–Y. Gao, W. Liu, R.–L. Tang, *Inorg. Chem.*, 2025, **64**, 3643–3648.
43. S.–K. Kurtz, T.–T. Perry, *J. Appl. Phys.*, 1968, **39**, 3798–3813.
44. T. Chen, Z. Sun, X. Liu, J. Wang, Y. Zhou, C. Ji, S. Zhang, L. Li, Z.–N. Chen, J. Luo, *J. Mater. Chem. C.*, 2014, **2**, 8723–8728.
45. D. Yan, M.–M. Ren, F.–F. Mao, Y. Ma, R.–L. Tang, B. Zhang, Y. Ma, X.–D. Zhang, S.–F. Li, *Inorg. Chem.*, 2023, **62**, 1323–1327.
46. L. Zhang, X. Zhang, F. Liang, Z. Hu, Y. Wu, *Inorg. Chem.*, 2023, **62**, 14518–14522.
47. X. Li, P. Gong, M. Chen, S. Zhuang, M. Qi, W. Wang, X. Wang, Z. Jia, M. Xia, *Inorg. Chem. Front.*, 2025, **12**, 7675–7683.
48. L. Li, H. Wu, H. Yu, Z. Hu, J. Wang, Y. Wu, *Mater. Today Chem.*, 2024, **42**, 102417.
49. J. Wu, Y.–F. Fu, W. Liu, and S.–P. Guo, *Inorg. Chem. Front.*, 2024, **11**, 7090–7097.
50. J. Lu, Y.–K. Lian, L. Xiong, Q.–R. Wu, M. Zhao, K.–X. Shi, L. Chen, L.–M. Wu, *J. Am. Chem. Soc.*, 2019, **141**, 16151–16159.
51. R. W. Godby, M. Schluter and L. J. Sham, *Phys. Rev. B: Condens. Matter Mater. Phys.*, 1987, **36**, 6497–6500.
52. J. P. Perdew, Y. Wang, *Phys. Rev. B.*, 1992, **45**, 13244–13249.
53. M. J. Dodge, *Appl. Opt.*, 1984, **23**, 1980–1985.
54. D. E. Zelmon, D. L. Small, D. Jundt, *J. Opt. Soc. Am. B.*, 1997, **14**, 3319–3322.



Data Availability StatementView Article Online
DOI: 10.1039/D6SC00466K

- The data supporting this article have been included as part of the Supplementary Information.
- Crystallographic data for $C_4H_{13}N_5Cl_2$ and $(C_4H_{13}N_5)ZnCl_4$ has been deposited with the CCDC numbers of 2521794 and 2522224 respectively.

